

## Groundwater Potential Assessment in the Upper Oum Er-Rbia Basin, Northern Morocco

Abdelbaset Midaoui<sup>1\*</sup>, Malika El-Hamdouny<sup>2</sup>, Abdenbi Elaloui<sup>1</sup>,  
Morad Karroum<sup>1</sup>, Abdelghani Boudhar<sup>1</sup>, Abderrahim Lahrach<sup>2</sup>

<sup>1</sup> Data Science for Sustainable Earth Laboratory, Sultan Moulay Slimane University, Beni Mellal 23000, Morocco

<sup>2</sup> Laboratoire d'Ecologie Fonctionnelle et Génie de l'Environnement, Sidi Mohamed Ben Abdellah University, Fez 30000, Morocco

\* Corresponding author's e-mail: a.midaoui@usms.ma

### ABSTRACT

This study aimed to assess the groundwater potential zones (GWPZ) in northern Morocco's Upper Oum Er-Rbia Basin (UOER). In such a semi-arid context, groundwater resources are crucial to sustaining essential human activities, but they are under stress due to increased overuse and climate change. This investigation utilized remote sensing in a GIS framework along with a multi-criteria decision analysis (MCDA) technique using the analytic hierarchy process (AHP) for the first time in this region. Ten thematic layers were created, representing the most significant parameters, which were then weighted and overlaid. The output map shows five levels of potential: very low, low, medium, high, and very high, covering 12%, 19%, 20%, 27%, and 22% of the basin area, respectively. Comparing the assessment results to the borehole yield, the AUC-ROC curve showed a value of 84.5%, which testifies to the excellent performance of the methodology used. Of the 10 criteria used, lithology was shown to be the most significant factor, followed by LULC, slope, and geomorphology. The study results offer an extensive insight into the hydrogeological potential of the UOER basin. These findings are essential for decision-makers and encourage the efficient utilization of groundwater resources, thus supporting broader objectives of sustainable development.

**Keywords:** groundwater potential, MCDA, AHP, remote sensing, upper Oum Er-Rbia.

### INTRODUCTION

Groundwater is essential for maintaining human activities in rural regions, especially in arid and semi-arid climates. It provides water for drinking, irrigation, and a number of other applications, making it a necessary resource for home, industrial, and agricultural usage [Yifru et al., 2020; Zamani et al., 2022]. However, the sustainability of this priceless resource is being threatened by the growing problems of over-exploitation and the effects of climate change [Deshmukh et al., 2022; Mays, 2013]. Morocco, a country with a high reliance on groundwater, is vulnerable to depletion and deterioration of this resource [Hssaisoune et al., 2020]. The country is heavily dependent on groundwater, which provides 60% of its total water supply [Oudra and

Talks, 2019], mainly for the support of agricultural operations and the provision of drinking water to isolated rural populations (douars). Additionally, Morocco is dealing with a serious water issue that has been made worse by a number of causes, including population increase, urbanization, economic development, climatic unpredictability and change, and insufficient governance and management. Agricultural runoff, industrial effluents, and home wastewater also overuse as well as contaminate many aquifers [World Bank Group, 2017]. The World Bank estimates that Morocco's renewable water resources per capita have decreased by almost 60% since 1960 [World Bank Group, 2021]. In this regard, a comprehensive examination of the existing and projected situation of groundwater resources in Morocco is of the utmost importance, along with the investigation of viable

adaptation techniques for long-term groundwater management [Mays, 2013; Megdal, 2018]. One of the most vulnerable areas in the Moroccan Atlas Mountains is the Upper Oum Er-Rbia basin. In this semi-arid area, groundwater resources provide water for drinking and agriculture, but they are under a lot of stress because of overuse and the effects of climate change [Chaponniere and Smakhtin, 2006]. Geophysical surveys and reconnaissance drilling are two common conventional approaches for assessing groundwater potential, although they can be expensive [K. K. Mandal et al., 2021] and may not offer sufficient geographical coverage for a thorough assessment [Arulbalaji et al., 2019]. Furthermore, the data obtained from the hydraulic basin agency reveal that 60% of the boreholes dug in the UOER are dry, proving that further research is needed to fully reveal the region’s hydrogeological potential. This research suggests the use of the innovative approach that combines multi criteria decision analysis (MCDA), remote sensing methods, and the Analytic Hierarchy Process (AHP) within a GIS framework to bridge this knowledge gap and promote sustainable groundwater management in the UOER region [Hussein et al., 2017; Yifru et al., 2020]. The combination of GIS and remote sensing data has become a useful tool in multiple scientific fields [Chaminé et al., 2021]. Remote sensing provides crucial spatial information that can largely improve the awareness of groundwater potential distribution [Abdalla et al., 2020; Lentswe and Molwalefhe, 2020]. The purpose of

this study was to evaluate the effectiveness and efficiency of the MCDA, remote sensing, and AHP methods in assessing groundwater potential in semi-arid regions with data scarce, like the UOER. Many previous studies have shown promising results when the AHP technique is applied in a GIS-based approach along with other geospatial technologies [Al Garni and Awasthi, 2017; Ouma and Tateishi, 2014]. These integrative applications have successfully defined groundwater potential zones and produced realistic potential maps that can serve as a base for efficiently managing groundwater and well-informed planning [Achu et al., 2020; Saravanan et al., 2020].

## MATERIALS AND METHODS

### Area of interest

The area of interest corresponds to the UOER basin, with its outlet at the Ahmed El Hansali dam (Fig.1). It encompasses a portion of the southwest of the Middle Atlas dominated by Jurassic carbonates and the east of the Central Massif marked by Visean flysch and wildflysch [Bamoumen et al., 2008; Bouabdelli and Piqué, 1996]. The zone falls mostly within the administrative provinces of Khenifra and Ifrane. Spanning from latitudes 32° 32' N to 33° 12' N and longitudes 5° 4' W to 5° 55' W, the area covers 3383 km<sup>2</sup>. Elevations range from 600 m at the dam outlet to 2400 m upstream in the Jbel Hayane ridge. The basin is drained by the Oum Er-Rbia River, originating as the Oued

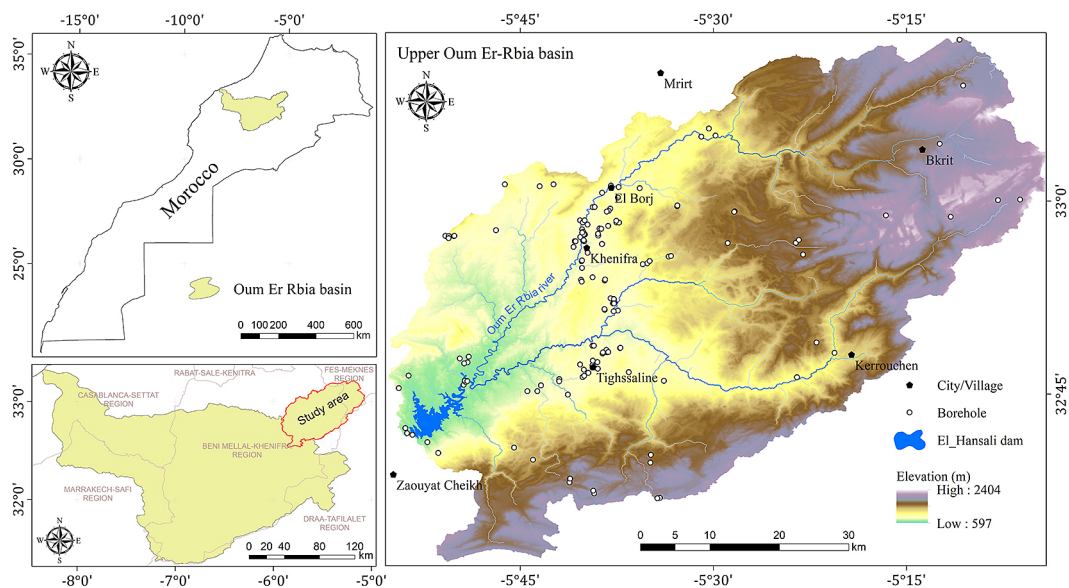


Figure 1. The upper Oum Er-Rbia basin’s location

Fellat and flowing towards the El Hansali dam in a general northeast to southwest direction, receiving contributions from various left-bank tributaries, notably the Oued Serou. The western areas covered by impermeable Paleozoic shales and the Oued Serou valley, composed of Permo-Triassic clay and basaltic dolerites, exhibit low hydrogeological potential. Conversely, the Jurassic carbonate regions display significantly better potential. The area experiences a Mediterranean mountain climate, with average minimum winter temperatures around -5 °C and summer maximum temperatures reaching approximately 40 °C. Annual rainfall averages 666 mm [Faouzi et al., 2022], and prevalent soil types include Rendzinas and Chromic Luvisols of medium texture [FAO-UNESCO, 1977].

### Methodological approach

To characterize Groundwater potential zones (GWPZ), a comprehensive set of influencing factors were employed. These factors spanned geological, geographical, pedological, topographical, and hydro-climatic aspects. Tomas Saaty’s analytic hierarchy process [1980] served as the method for weighted overlay multicriteria decision analysis (MCDA) in a GIS environment (Fig.2). This approach was applied for the first time in the UOER Basin. Literature review demonstrates the high efficiency of this method in defining GWPZ [Taher et al., 2023]. The MCDM-AHP approach is widely used for groundwater potential delineating

[Mallick et al., 2019; Shao et al., 2020]. The scientific community recognizes AHP to be a reliable and practical multicriteria analysis method used to resolve challenging decision-making situations [Al Garni and Awasthi, 2017; Machiwal et al., 2011].

### Selection of parameters

The MCDA approach can involve numerous geoenvironmental parameters in order to delineate the GWPZ. The selection of those affecting significantly groundwater recharge and storage is a significant step [Trabelsi et al., 2022]. A literature review of recently published papers focusing on hydrogeological potential [Mallick et al., 2019; Patra et al., 2018] was conducted in order to identify the most relevant parameters. Ten most rated factors – lithology, land use/cover, slope, geomorphology, rainfall, density of lineament, density of drainage, soil texture, TWI, and curvature – were retained for this study.

### Thematic layers preparation and data used

To prepare a thematic layer for each influencing parameter, data were collected from multiple sources (Table 1). These datasets were mainly processed using ArcGIS. Other software was used, notably Geomatica to extract lineaments from Landsat images and Google Earth Engine to extract rainfall and LULC data. All thematic layers are transformed into raster with the same spatial

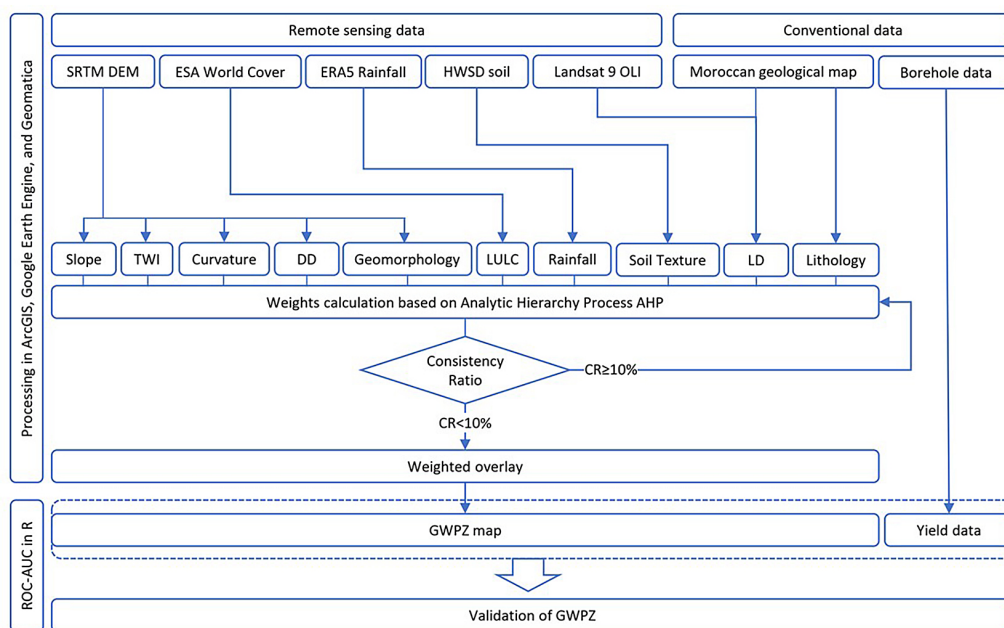


Figure 2. Methodological flowchart used to delineate GWPZ in the upper Oum Er-Rbia basin

**Table 1.** Sources of data used in the study

Data	Source	Thematic layer
SRTM DEM 30 m	NASA (Earthdata)	slope, TWI, curvature, drainage density, geomorphology
ESA World Cover 10 m v 200	European Space Agency extracted from Google Earth Engine	LULC
ERA5 Rainfall 0.1° × 0.1° resolution	Copernicus program extracted from Google Earth Engine.	rainfall
HWSD soil v 1.2 1:5,000,000	FAO/UNESCO	soil texture
Landsat 9 OLI	USGS earth explorer	lineament density
Geological map 1:1,000,000	Moroccan geological map	lithology, lineament density
Borehole data	The Oum Er-Rbia Hydraulic Basin Agency	yield data from 124 boreholes for validation

resolution (30×30 meters), allowing weighted superposition. Additionally, they were reprojected using the same coordinate system (WGS84) and reclassified into five classes.

Lithology was created in ARCGIS based on the Moroccan geological map. LULC was extracted from ESA WorldCover 10m v200 product [Zanaga et al., 2022], in Google Earth Engine. Soil data was extracted directly from the Harmonized World Soil Database [FAO and IIASA, 2023].

Slope was generated in ArcGIS using the STRM DEM. The default method “PLANAR” of the *Slope* tool was used. It consists of measuring the maximum difference between the central cell and its eight neighbors, using a 3 by 3 cell neighborhood moving window. Equation (1) calculates the slope in degree.

$$Slope = \tan^{-1} \sqrt{((dz/dx)^2 + (dz/dy)^2)} \times (180/\pi) \quad (1)$$

where:  $dz/dx$  expresses the change in the horizontal direction, and  $dz/dy$  in the vertical direction.

Geomorphology was automatically generated based on the SRTM DEM. Weiss [2001] described an automated GIS method for landform classification, based on the Topographic Position Index (TPI), widely used for this purpose [Abdekareem et al., 2022]. Equation (2) show how the *TPI* is derived from DEM, by calculating the difference in altitude between each cell and the mean in a predetermined neighborhood cells [De Reu et al., 2013].

$$TPI = z_0 - \frac{1}{n} \sum_{i=1}^n z_i \quad (2)$$

where:  $z_0$  and  $z_i$  represent the DEM value in a cell and the average of neighboring cells, respectively, and  $n$  is the number of neighborhood cells in predefined radius.

Negative *TPI* means negative terrain like valleys and Canyons, null or low values represent flat areas or constant slopes, while positive *TPI* means positive terrain like ridges and mountains. The combination of this topographic index at a small and large scale helps to distinguish a diversity of landforms [Weiss, 2001].

Rainfall was extracted from ERA5-Land monthly aggregated data, specifically from total\_precipitation\_sum band [Muñoz Sabater, 2019] in Google Earth Engine. The latest 32-year series (1990–2022) was used to elaborate an average annual precipitation map. Using ArcGIS functions, precipitation values were extracted from each grid cell center and then interpolated using the IDW method [Rahman et al., 2022] to obtain the average annual precipitation map.

Drainage density layer was created in the ArcGIS software [Abdullahi et al., 2023]. Stream network was generated based on DEM using Hydrology tools. then line density tool served to calculate the density of drainage for each cell based on Eq. (3). Drainage density (km/km<sup>2</sup>) in a cell consists of dividing the total line stream’s length  $D_i$  (km) inside a given radius by the area  $A$  (km<sup>2</sup>).

$$DD = \sum \frac{D_i}{A} \quad (3)$$

Lineament density layer was prepared in two steps. First, lineaments were extracted automatically using Geomatica software [Ozegin et al., 2023]. Linear and sublinear structures can be recognized on satellite images [Arulbalaji et al., 2019]. The Landsat 9 OLI product was used in this process to extract lineaments. Then, the obtained result was checked and completed based on the geological

map in ArcGIS before establishing the lineament density layer (km/km<sup>2</sup>) in the same way as the DD map, employing the Line Density Tool.

Curvature was created by calculating the second derivative of the DEM surface in ArcGIS [Kumar et al., 2023; Moore et al., 1991]. Positives values of curvature mean a convex land surface, while negative values mean a convex land surface [Ghosh et al., 2022]. TWI was calculated in a GIS environment based on DEM using Eq. (4).

$$TWI = \ln(F_a / \tan \beta) \tag{4}$$

where:  $F_a$  is the flow accumulation (upslope area), and  $\beta$  is the local slope.

### Weighting using AHP

The weighting of the different thematic layers is a decisive step in multi-criteria analysis. The objective is to attribute weights to criteria and sub-criteria according to their importance in determining the problem. One popular method that has served in various GIS-based multicriteria analyses is AHP [Ghosh et al., 2022] developed by Saaty [1980]. The principle is to create a matrix for pair-wise comparison by combining the different criteria according to expert opinions [Ifediegwu, 2022; Saaty, 1990]. The intricate MCDA with many criteria is reduced to one level [Ifediegwu, 2022], with each pair of criteria handled independently. In other words, the Analytic Hierarchical Process breaks down the complex analysis into many simple ones at hierarchical levels and gives the criterion weight [Al Garni and Awasthi, 2017]. The importance of each criterion was determined according to the Saaty significance scale (Table 2), based on the weights allocated in numerous previous studies. Table 3 gives the resultant pair-wise comparison matrix. Then, the normalized weights are calculated utilizing the criteria’s geometric mean

**Table 2.** Relative importance scale [Saaty, 1980]

Intensity of importance	Definition
1	Equal importance
3	Weak importance of one over another
5	Essential or strong importance
7	Demonstrated importance
9	Absolute importance
2,4,6,8	Intermediate values between two adjacent judgments

of matrix rows. The five classes or categories of each criterion received a rank from 1 to 5, proportional to their degree of influence on the hydrogeological potential [Castillo et al., 2022; Saravanan et al., 2020]. The weight given to the criteria as thematic layers and the ranks attributed to the sub-criteria are shown in Table 4. To evaluate the analysis’s robustness, the consistency ratio was calculated using Saaty’s derivation, as is provided in Eq. (5).

$$CR = \frac{CI}{RCI} \tag{5}$$

where:  $RCI$  – the Saaty’s random consistency index (Table 5),  $CI$  – the consistency index given in Eq. (6).

$$CI = \frac{\lambda_{max} - n}{n - 1} \tag{6}$$

where:  $\lambda_{max}$  – the principal Eigenvalue, and  $n$  – the number of criteria.

With ten criteria considered, a CR less than or equal to 10% is satisfactory [Saaty, 1990]. If the consistency ratio exceeds this threshold, then anomalies in the pair-wise comparison must be identified and adjusted [Machiwal et al., 2011; Yifru et al., 2020]. In this study, a satisfactory consistency ratio  $CR = 3.8\%$  was obtained.

**Table 3.** Resulting pair-wise comparison matrix

Criteria	Lith	LULC	S	G	R	DD	LD	ST	TWI	C
Lithology (Lith)	1	3	4	4	4	5	5	6	7	8
LULC	1/3	1	1	1	2	3	3	3	6	7
Slope (S)	1/4	1	1	1	1	2	3	3	6	7
Geomorphology (G)	1/4	1	1	1	1	2	2	3	6	6
Rainfall (R)	1/4	1/2	1	1	1	1	2	2	6	6
Drainage density (DD)	1/5	1/3	1/2	1/2	1	1	1	1	5	6
Lineament density (LD)	1/5	1/3	1/3	1/2	1/2	1	1	1	5	6
Soil texture (ST)	1/6	1/3	1/3	1/3	1/2	1	1	1	5	6
TWI	1/7	1/6	1/6	1/6	1/6	1/5	1/5	1/5	1	2
Curvature (C)	1/8	1/7	1/7	1/6	1/6	1/6	1/6	1/6	1/2	1

### Delineation of GWPZ

The ten thematic maps, already prepared and weighted, were overlaid and aggregated using a linear combination to define groundwater potential [Tiwari et al., 2019]. The analysis was implemented owing to the weighted overlay tool in ArcGIS, according to Eq. (7).

$$GWPZ = \sum_{i=1}^n \sum_{j=1}^m (W_i \times r_j) \quad (7)$$

where:  $W_i$  – the weight of the  $i$  – th criterion, and  $r_j$  the rank of the  $j$ -th sub-criterion.

### Validation of GWPZ

The validation of the groundwater potential zones can be done based on hydrogeological measured data, such as wells yield [Rahmati et al., 2015; Thapa et al., 2018] or groundwater level [Patra et al., 2018; Pradhan et al., 2021].

**Table 4.** Weights attributed to criteria and sub-criteria influencing groundwater potential

Criterion	Weight (W <sub>i</sub> )	Sub-criterion	Rank (r <sub>j</sub> )
Lithology	31.31	Cretaceous red detrital facies	3
		Quaternary alkaline basalts	5
		Jurassic carbonates	5
		Eocene limestone and red gypsum marls	4
		Triassic basalt	2
		Triassic red clay	1
		Permian detrital facies	3
		Visean limestone and flysh	4
		Quaternary alluvium	4
		Ordovician schists	1
		Devonian schists with limestone and sandstone beds	1
		Cambrian–Ordovician schists and sandstones	1
		Precambrian and paleozoic rhyolite	1
		Jurassic red sandstone	4
LULC	13.82	Tree cover	4
		Shrubland	4
		Grassland	3
		Cropland	4
		Built-up	1
		Bare/sparse vegetation	2
		Waterbodies	5
Slope	12.03	00 – 05	5
		05 – 10	4
		10 – 15	3
		15 – 25	2
		25 – 60	1
Geomorphology	11.31	Canyons, deeply incised streams	5
		Midslope drainages, shallow valleys	5
		Upland drainages, headwaters	4
		U-shaped valleys	4
		Plains	3
		Open slopes	3
		Upper slopes, mesas	2
		Local ridges/hills in valleys	2
		Midslope ridges, small hills in plains	1
		Mountain tops, high ridges	1

**Table 4. Cont.**

Rainfall	9.47	492 – 530	1
		531 – 560	2
		561 – 590	3
		591 – 620	4
		621 – 680	5
Drainage density	6.67	0.00 – 0.25	5
		0.26 – 0.66	4
		0.67 – 1.13	3
		1.14 – 1.86	2
		1.87 – 3.18	1
Lineament density	6.03	0.00 – 0.36	1
		0.37 – 0.60	2
		0.61 – 0.86	3
		0.87 – 1.16	4
		1.17 – 1.97	5
Soil texture	5.75	Chromic Luvisols fine textured	1
		Rendzinas medium textured	3
		Chromic Luvisols medium textured	4
TWI	2.01	02.78 – 05.76	1
		05.77 – 07.38	2
		07.39 – 09.68	3
		09.69 – 13.26	4
		13.27 – 24.50	5
Curvature	1.59	-10.89 to -0.89	1
		-0.88 to -0.26	2
		-0.25 to 0.36	3
		0.37 to 1.08	4
		1.09 to 11.88	5

**Table 5.** Random consistency Index RCI depending on number of criteria n [Lentswe and Molwalefhe, 2020]

n	3	4	5	6	7	8	9	10
RCI	0.58	0.9	1.12	1.24	1.32	1.41	1.45	1.49

The Hydraulic Basin Agency has made the data from 124 boreholes distributed in the upper Oum Er-Rbia basin (Fig. 1) available for research. Using their coordinates, the boreholes were plotted on the obtained map (Fig. 9) to compare the estimated hydrogeological potential and observed yield. To measure the potential map accuracy, the Area Under the Receiver Operating Characteristic Curve (AUC-ROC) was used under R. The AUC-ROC curve is widely used to evaluate the accuracy in this kind of prediction [Das and Pal, 2019; Trabelsi et al., 2022]. The ROC curve is established based on

the confusion matrix. The true positive rate, or sensitivity, represents the ordinates, while the false positive rate, or 1-specificity, represents the abscissas [Shailaja et al., 2019; Trabelsi et al., 2022]. Then, the area under the ROC curve is calculated. It reveals the model’s precision through its capacity to predict the occurrence of an event correctly [El Jazouli et al., 2019; Rahmati et al., 2015]. The AUC varies from 0.5 when the prediction is completely random to 1 when the prediction is perfect [Trabelsi et al., 2022; Yesilnacar and Topal, 2005]. Intermediate performances are given in Table 6.

## RESULTS AND DISCUSSION

### Thematic maps

#### Lithology

The hydrogeological potential is fundamentally linked to the lithological nature of the terrain. The hydrogeological properties of aquifer materials are mainly defined by their lithology [Morgan et al., 2023]. Rock characteristics like porosity and permeability control water movement and storage [Mandal K.K. et al., 2021; Thapa et al., 2018]. The facies that present great hydrogeological potential, such as carbonates, Quaternary basalts, alluvium, and sands, received significant weight, while the lowest weights were attributed to unfavorable formations, such as clays and schists (Table 4). Fourteen geological units were distinguished (Fig. 3). The most dominant formation is the Middle Jurassic carbonates, which cover almost half of the basin area (approximately 1473 km<sup>2</sup>). The Viséan Flysch and the Triassic basalts cover 12% each; the Triassic red clays occupy 9%; the Cretaceous red detrital facies and the Ordovician schists cover 6.8% each. About 10% of the basin area is shared between Eocene limestone and marls, Quaternary basalts, Cambrian-Ordovician schists and sandstones, Permian detrital facies, Quaternary alluvium, Devonian schists, Precambrian and Paleozoic rhyolite, and Jurassic sandstone.

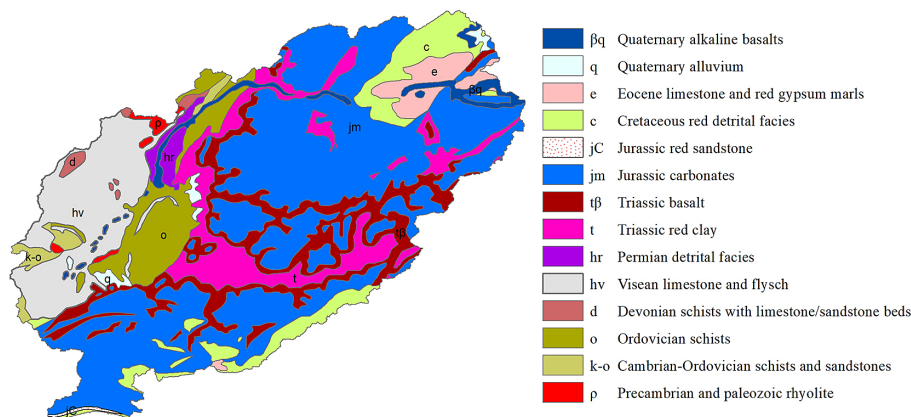


**Figure 3.** Lithological map of the upper Oum Er-Rbia basin (source: geological map of Morocco at 1:1,000,000)

**Table 6.** Model performance according to the AUC value [Rahmati et al., 2015]

AUC values	0.5 – 0.6	0.6 – 0.7	0.7 – 0.8	0.8 – 0.9	0.9 – 1
Model performance	poor	average	good	very good	excellent

#### LULC

While land cover describes natural features like forests and water bodies, land use relates to human activities like settlement, roads, and industries [Mandal K.K. et al., 2021]. LULC influences groundwater recharge [Mengistu et al., 2022; Salem et al., 2023]. It determines evapotranspiration, runoff, and infiltration rates [Anusha et al., 2022; Yadav et al., 2023]. The built-up land was given the lowest ranking, while the highest rank was attributed to the waterbodies (Table 4) [Anusha et al., 2022]. The LULC map consists of grassland 41.7%, tree cover 29.4%, cropland 17.4%, shrubland 8.9%, bare/sparse vegetation 1.9%, waterbodies 0.5%, and built-up 0.4% (Fig. 4a).

#### Slope

The steepness of the slope has a significant impact on two important hydrological processes: surface runoff and infiltration [Mandal K.K. et al., 2021]. Flat areas increase the accumulation and infiltration of water [Castillo et al., 2022]. Conversely, the areas with steep slopes experience lower infiltration and higher surface runoff [Allafta et al., 2021; Sutradhar et al., 2021]. Thus, the weights attributed are inversely proportional to the slope values. The slope in the UOER basin ranges from 0 to 60° (Fig.4b). Zonal statistics reveal that 95% of the area has a slope greater than 5°. Flat terrains (0 to 5°) are located essentially in the Central Massif part of the basin in the west and the Bekrit syncline in the north. The steepest slopes (25 to 60°) cover

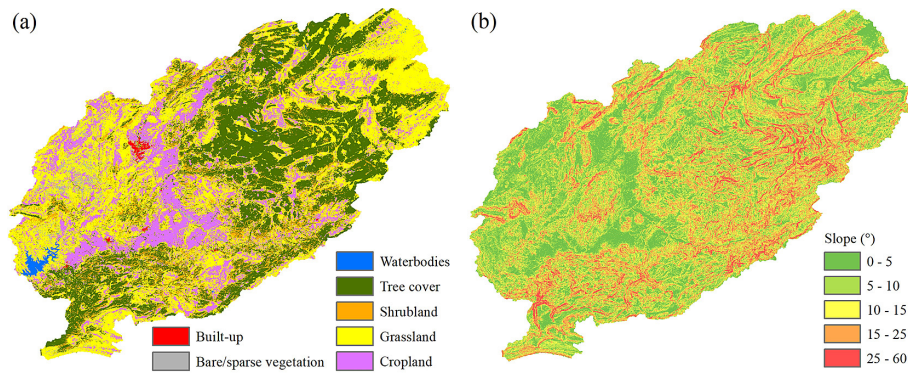


**Figure 4.** Land use/land cover (a) and slope (b) in the UOER basin

28% of the basin area, which coincides with the ridges of the Middle Atlas range.

### Geomorphology

Geomorphology depicts landforms resulting from internal and external geological phenomena [Aslan and Çelik, 2021]. It depends on the structural evolution of geological formations [Duguma, 2023], weathering, and erosion processes. Landforms influence the percolation towards the impermeable layer [Radulović et al., 2022]. It significantly affects the groundwater movement and recharge [Upwanshi et al., 2023]. Plains and valleys are favorable to infiltration, which increases groundwater potential [Muavhi et al., 2022]; hence, they received high weights. Conversely, hills and ridges are unfavorable regions; they receive low weights (Table 4). Examination of the obtained map (Fig. 5) shows a predominance of open slopes, covering 41% of the study area, followed by plains at 16%, and upper slopes/mesas at 9%. Midslope drainages/shallow valleys, midslope ridges/small hills in plains, and U-shaped valleys cover 8% each. Mountain tops/high ridges, and canyons/deeply incised streams occupy 5% each. Finally, upland drainages/headwaters and local ridges/hills in valleys cover < 1% each.

### Rainfall

The rainfall has a direct effect on the groundwater potential and recharge in a particular area [Chaudhry et al., 2021; Rahman et al., 2022]. This, in turn, affects the hydrogeological conditions of that area [Masroor et al., 2023]. The more it rains, the higher the groundwater potential; hence, a rank is assigned accordingly (Table 4). The map in Figure 6a indicates that the mean annual precipitation in the basin range from 492

to 680 mm. These variations are explained by topography and altitude. High values (from 590 to 680 mm) are observed in the North and South, covering almost one-third (1106 sq. km) of the study area. Conversely, low rainfall values (less than 560 mm) cover 39% of the basin's area (1318 sq. km) in the East and West regions.

### Drainage density

Drainage density (DD) represents the density of streamline in the basin. It is calculated as the ratio of stream lengths to area [Yadav et al., 2023]. DD is inversely related to groundwater [Singha et al., 2021]. High DD suggests low infiltration and, thus, poor groundwater potential. Conversely, the areas with low DD suggest high groundwater potential [Masroor et al., 2023]. Therefore, the assigned rank decreases when the DD increases [Anusha et al., 2022] (Table 4). Figure 6b shows that the DD is between 0 and 3.18 km/km<sup>2</sup>. The map shows five classes: 0–0.25, 0.26–0.66, 0.67–1.13, 1.14–1.86, and 1.87–3.18, covering areas of 1406 sq. km (42%), 851 sq. km (25%), 646 sq. km (19%), 398 sq. km (12%), and 82 sq. km (2%), respectively.

### Lineament density

Lineaments designate linear or curvilinear surface structures that are structurally controlled and reflect underground fractures or faults [Arulbalaji et al., 2019]. These increase secondary porosity and permeability [Hussein et al., 2017; Mandal P. et al., 2021], which facilitates infiltration. As a result, they have an important influence on the movement and storage of groundwater [Castillo et al., 2022]. Greater lineament density (LD) values signify increased recharge and, hence, enhanced hydrogeological potential [Tiwari et al.,

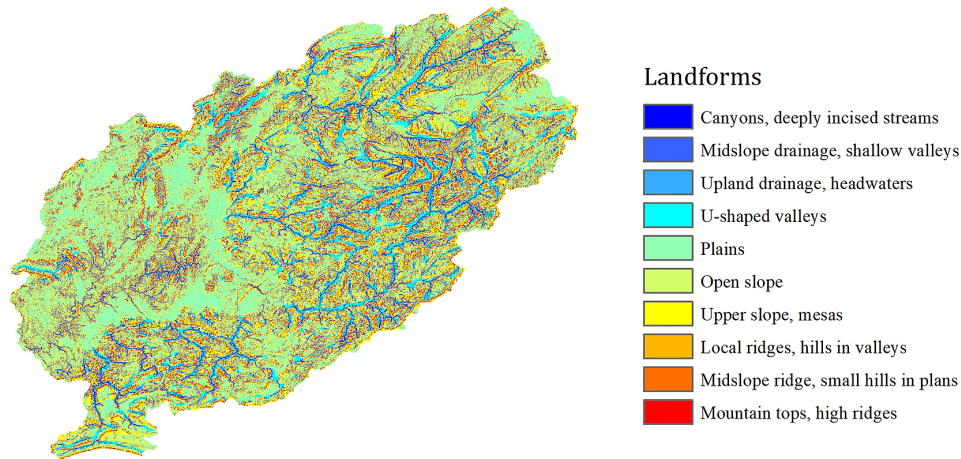


Figure 5. Geomorphic unit distribution in the upper Oum Er-Rbia basin

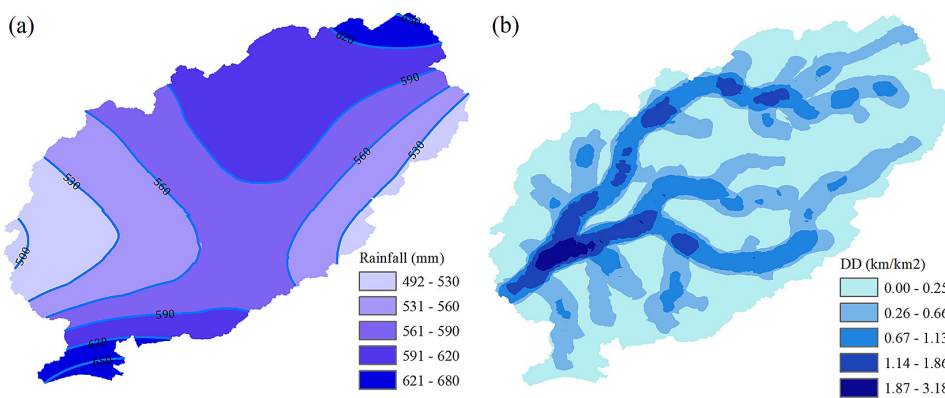


Figure 6. Rainfall (a) and drainage density (b) in the upper Oum Er-Rbia

2019]. Therefore, high-density classes received a high rank, and low-density classes were assigned a low rank (Table 4). The LD values in the basin are between 0 to 1.97 km/km<sup>2</sup>. Figure 7a shows five classes of LD: 0–0.36, covering 20% of the basin’s area; 0.37–0.6 (27%); 0.61–0.86 (23%); 0.87–1.16 (19%) and 1.17–1.97 (10%).

#### Soil texture

Depending on its texture, the soil regulates how much water may reach underlying formations, which affects groundwater recharge [Anusha et al., 2022; Morgan et al., 2023]. Groundwater availability depends on the saturation level of the vadose zone, which is affected by soil texture [Arulbalaji et al., 2019; Mandal K.K. et al., 2021]. Thus, coarse-textured soils will receive a high ranking, while fine-textured soils will receive a low ranking. The map (Fig. 7b) displays three soil units, with the Rendzinas medium-textured unit being the most dominant, covering an area of 2101 km<sup>2</sup> (62%). The Chromic Luvisols medium-textured unit has

an area of 1099 km<sup>2</sup> (32%), while the Chromic Luvisols fine-textured unit covers 183 km<sup>2</sup> (5%).

#### TWI

TWI, or topographic wetness index, reflects the impact of topography on the amount of runoff generated and flow accumulation [Morgan et al., 2023; Yadav et al., 2023]. This index is used here to consider the part of topography in conditioning infiltration [Castillo et al., 2022; Upwanshi et al., 2023]. TWI is positively correlated to groundwater potentials; a high rank was attributed to high values of TWI, and vice versa [Abdekareem et al., 2022; Castillo et al., 2022]. The obtained map (Fig. 8a) was classified into five categories: 2.78–5.76 (36% of the study area), 5.77–7.38 (40%), 7.39–9.68 (16%), 9.69–13.26 (16%), and 13.27–24.5 (2%).

#### Curvature

The concept of curvature refers to the change in slope of a surface [Morgan et al., 2023]. It reflects the concavity or convexity of the surface

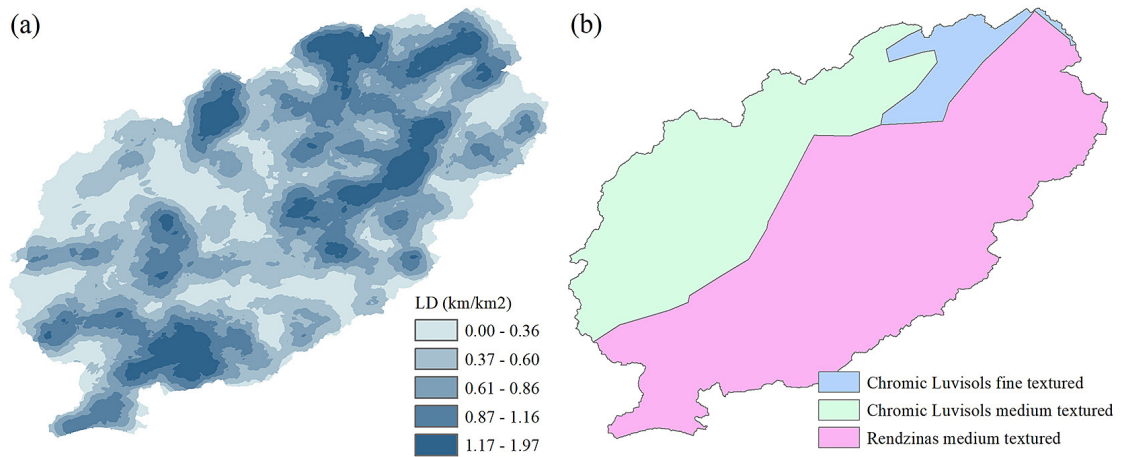


Figure 7. Lineament density (a) and soil texture (b) in the study area

profile upwards. [Upwanshi et al., 2023]. The areas with concave and flat surfaces tend to retain more water and have a greater infiltration capacity compared to the areas with convex surfaces [Abdekareem et al., 2022]. Therefore, the convex areas (high curvature values) received high rank, and the concave areas (low curvature values) were given low rank. The obtained map (Fig.8b) shows a slightly equal percentage of concave and convex surfaces. The curvature classes are as follows: -10.89 to -0.89, which covers 6% of the area; -0.88 to -0.26, which covers 21%; -0.25 to 0.36, which covers 46%; 0.37 to 1.08, which covers 23%; and 1.09 to 11.88, which covers 4%.

### Groundwater potential zones map

Figure 9 presents the groundwater potential map in the upper Oum Er-Rbia basin. The results show an index of potential ranging from 1.4 to 4.72, which has been classified into 5 classes:

Very low potential 1.4–2.51 covering 417 sq. km (12%), low potential 2.52–2.96 covering 626 sq. km (19%), medium potential 2.97–3.39 covering 678 sq. km (20%), high potential 3.4–3.78 covering 907 sq. km (27%), and very high potential 3.79–4.72 covering 746 sq. km (22%). The areas of high to very high potential are generally located on the Jurassic limestones of the Middle Atlas, in the north and in the extreme south, where precipitation is at its maximum. The areas with low and very low potential are generally located on impermeable lithological facies, to the west on the Paleozoic shales of central Morocco, and following the Wadi Srou valley, where Triassic red clays predominate. Moderate potential zones are located primarily on the limestone and flysch facies of the Viséan to the west, as well as on the cretaceous detrital facies in the extreme northeast and on a strip along the southern limit of the basin. This analysis proves that lithology, with a weight of 31.31, is the main factor controlling the groundwater

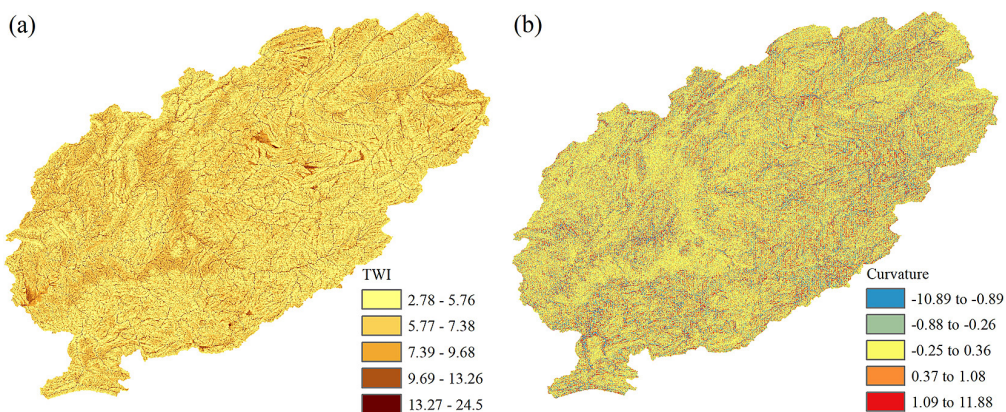
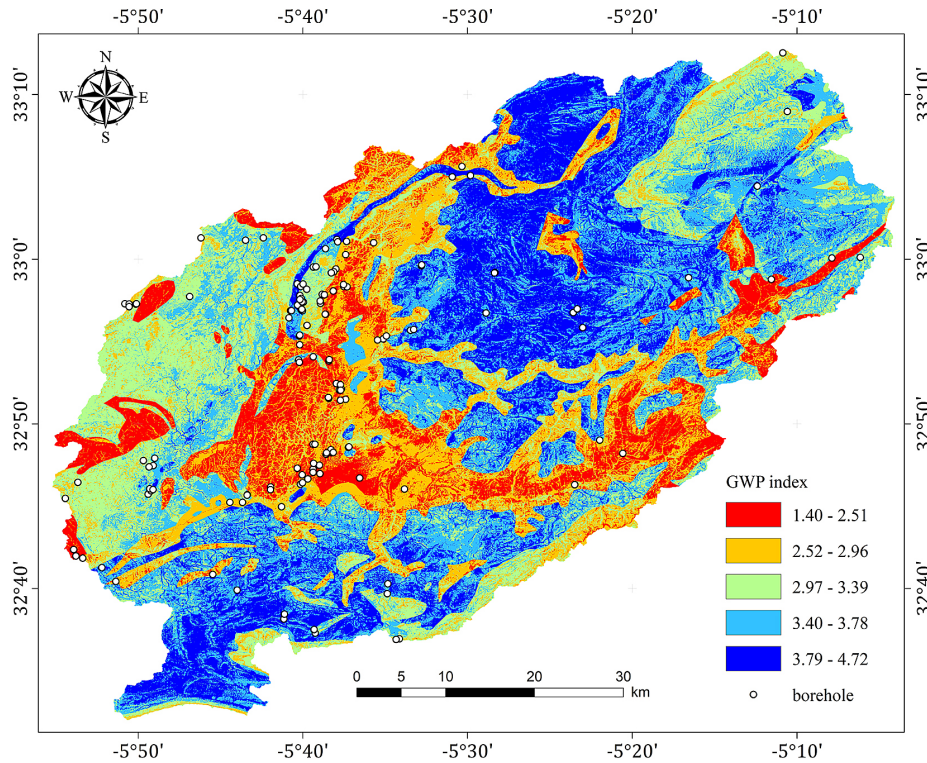


Figure 8. Topographic wetness index (a) and curvature (b) in the study area



**Figure 9.** Groundwater potential index and location of validation boreholes

occurrence in the study area [Castillo et al., 2022]. LULC, slope, and geomorphology were also considered important factors and received a weight of 13.82, 12.03, and 11.31, respectively. Rainfall, drainage density, lineament density, and soil texture were considered of moderate importance, and they received weights of 9.47, 6.67, 6.03, and 5.75, respectively. Finally, TWI and curvature received the least weight, with 2.01 and 1.59, respectively, as the weakest influencing factors.

**Validation**

Results have been validated based on borehole yield. The data on 124 boreholes in the study area was collected from the Oum Er-Rbia hydraulic basin agency. Most boreholes are concentrated near major agglomerations, such as Khenifra, El Borje, and Tighessaline (Fig. 1). However, these areas are located on Paleozoic shales, considered unfavorable for hydrogeological purposes, which explains why 60% of boreholes are dry. Thus, the spatial distribution is not necessarily an indicator of good potential. In the ArcGIS environment, the boreholes were superimposed on the obtained potential map. Then, a comparison of the predicted potential and borehole yield,

which range from 0 to 20 liters per second, was conducted in R. The AUC-ROC curve (Fig. 10) shows a prediction accuracy of 84.5%. On the basis of this result and according to Table 6, the MCDA approach with the AHP method used can be considered to have very good performance in this study (AUC in 0.8–0.9).

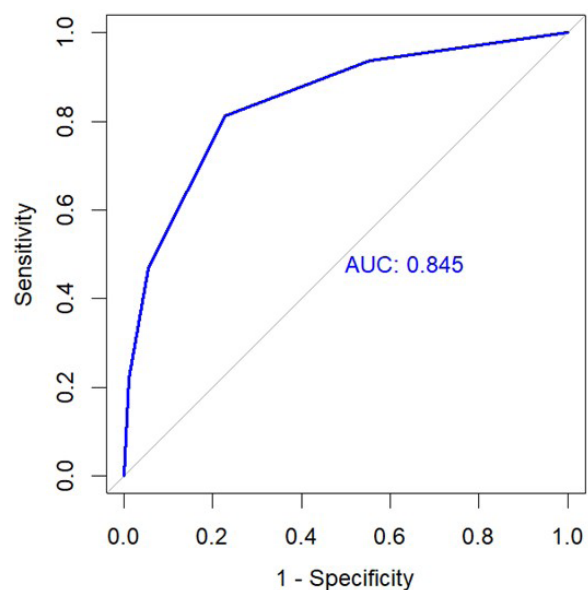


**Figure 10.** The AUC-ROC curve of validation based on yield data

## CONCLUSIONS

The water crisis throughout semi-arid and dry areas, like North Africa, has been worsened by the increasingly severe effects of climate change. The problem has been aggravated by inadequate management plans and strategies, as well as a lack of knowledge about water resources [Kumar et al., 2023]. This research tried to enhance the current knowledge on groundwater potential in the UOER basin, which could help improve water resource management. The main goal was to assess groundwater potential through an innovative and cost-effective approach that harnesses the power of MCDA, remote sensing, and AHP in a GIS framework. Hence, ten thematic layers representing the most influencing criteria were prepared, weighted, and superimposed in the ARCGIS environment. The obtained potential map generated based on this process was classified into five levels: very low, low, medium, high, and very high potential, covering 12%, 19%, 20%, 27%, and 22% of the study area, respectively. With an assigned weight of 31.31, lithology was deemed the most significant of the ten criteria employed in this investigation. Its effect on GWPZ was noticeable. LULC, slope, and geomorphology were weighed at 13.82, 12.03, and 11.31, respectively, and were also regarded as significant factors. Weighed at 9.47, 6.67, 6.03, and 5.75, respectively, soil texture, drainage density, rainfall, and lineament density were deemed to be of moderate importance. Lastly, the two factors that had the least weight were TWI and curvature, with respective values of 2.01 and 1.59. The validation based on yield, using the AUC-ROC curve, showed very good performance (84.5%). The results of the study provide a comprehensive understanding of the hydrogeological potential in UOER basin. The findings have the potential to support decision-making processes and promote the sustainable use of groundwater resources, aligning with broader sustainable development and land management objectives. The study can contribute to the good management of this precious resource, especially under the conditions of extreme shortage that Morocco is experiencing.

## Acknowledgements

The authors gratefully acknowledge the Oum Er-Rbia Hydraulic Basin Agency (ABHOER) for providing borehole data. They are also thankful to

USGS, NASA, ESA, FAO, and the Copernicus program for providing data to prepare thematic layers.

## REFERENCES

1. Abdalla F., Moubark K., Abdelkareem M. 2020. Groundwater potential mapping using GIS, linear weighted combination techniques and geochemical processes identification, west of the Qena area, Upper Egypt. *Journal of Taibah University for Science*, 14(1), 1350–1362. <https://doi.org/10.1080/16583655.2020.1822646>
2. Abdekareem M., Al-Arifi N., Abdalla F., Mansour A., El-Baz F. 2022. Fusion of Remote Sensing Data Using GIS-Based AHP-Weighted Overlay Techniques for Groundwater Sustainability in Arid Regions. *Sustainability (Switzerland)*, 14(13). <https://doi.org/10.3390/su14137871>
3. Abdullahi A., Jothimani M., Getahun E., Gunalan J., Abebe A. 2023. Assessment of potential groundwater Zones in the drought-prone Harawa catchment, Somali region, eastern Ethiopia using geospatial and AHP techniques. *Egyptian Journal of Remote Sensing and Space Science*, 26(3), 628–641. <https://doi.org/10.1016/j.ejrs.2023.07.005>
4. Achu A.L., Thomas J., Reghunath R. 2020. Multi-criteria decision analysis for delineation of groundwater potential zones in a tropical river basin using remote sensing, GIS and analytical hierarchy process (AHP). In *Groundwater for Sustainable Development*, 10. <https://doi.org/10.1016/j.gsd.2020.100365>
5. Al Garmi H.Z., Awasthi A. 2017. Solar PV power plant site selection using a GIS-AHP based approach with application in Saudi Arabia. *Applied Energy*, 206(September), 1225–1240. <https://doi.org/10.1016/j.apenergy.2017.10.024>
6. Allafta H., Opp C., Patra S. 2021. Identification of groundwater potential zones using remote sensing and GIS techniques: A case study of the shatt Al-Arab Basin. *Remote Sensing*, 13(1), 1–28. <https://doi.org/10.3390/rs13010112>
7. Anusha B.N., Pradeep Kumar B., Rajasekhar M., Raghu Babu K. 2022. Delineation of groundwater potential zones using geospatial and MCDM approaches in urban areas of Anantapur District, AP, India. *Urban Climate*, 46(March), 101341. <https://doi.org/10.1016/j.uclim.2022.101341>
8. Arulbalaji P., Padmalal D., Sreelash K. 2019. GIS and AHP Techniques Based Delineation of Groundwater Potential Zones: a case study from Southern Western Ghats, India. *Scientific Reports*, 9(1), 1–17. <https://doi.org/10.1038/s41598-019-38567-x>
9. Aslan V., and Çelik R. 2021. Integrated gis-based multi-criteria analysis for groundwater potential mapping in the euphrates's sub-basin, harran basin,

- turkey. *Sustainability* (Switzerland), 13(13). <https://doi.org/10.3390/su13137375>
10. Bamoumen H., Aarab E.M., Soulaïmani A. 2008. Tectono-Sedimentary and magmatic evolution of the Upper Viséan basins of Azrou-Khénifra and eastern Jebilet (Moroccan Meseta). *Estudios Geológicos*, 64(2), 107–122. <https://doi.org/10.3989/egeol.08642.020>
  11. Bouabdelli M., and Piqué A. 1996. Du bassin sur décrochement au bassin d'avant-pays: Dynamique du bassin d'Azrou-Khénifra (Maroc hercynien central). *Journal of African Earth Sciences*, 23(2), 213–224. [https://doi.org/10.1016/S0899-5362\(96\)00063-2](https://doi.org/10.1016/S0899-5362(96)00063-2)
  12. Castillo J.L.U., Cruz D.A.M., Leal J.A.R., Vargas J.T., Tapia S.A.R., Celestino A.E.M. 2022. Delineation of groundwater potential zones (GWPZs) in a semi-arid basin through remote sensing, GIS, and AHP approaches. *Water* (Switzerland), 14(13). <https://doi.org/10.3390/w14132138>
  13. Chaminé H.I., Pereira A.J.S.C., Teodoro A.C., Teixeira J. 2021. Remote sensing and GIS applications in earth and environmental systems sciences. *SN Applied Sciences*, 3(12), 870. <https://doi.org/10.1007/s42452-021-04855-3>
  14. Chaponniere A., Smakhtin V. 2006. A Review of Climate Change Scenarios and Preliminary Rainfall Trend Analysis in the Oum Er Rbia Basin, Morocco. 1–16.
  15. Chaudhry A.K., Kumar K., Alam M.A. 2021. Mapping of groundwater potential zones using the fuzzy analytic hierarchy process and geospatial technique. *Geocarto International*, 36(20), 2323–2344. <https://doi.org/10.1080/10106049.2019.1695959>
  16. Das B., and Pal S.C. 2019. Combination of GIS and fuzzy-AHP for delineating groundwater recharge potential zones in the critical Goghat-II block of West Bengal, India. *HydroResearch*, 2, 21–30. <https://doi.org/10.1016/j.hydres.2019.10.001>
  17. De Reu J., Bourgeois J., Bats M., Zwervaegher A., Gelorini V., De Smedt P., Chu W., Antrop M., De Maeyer P., Finke P., Van Meirvenne M., Verniers J., Crombé P. 2013. Application of the topographic position index to heterogeneous landscapes. *Geomorphology*, 186, 39–49. <https://doi.org/10.1016/j.geomorph.2012.12.015>
  18. Deshmukh M.M., Elbeltagi A., Kouadri S. 2022. Climate Change Impact on Groundwater Resources in Semi-arid Regions. In *Climate Change Impact on Groundwater Resources* (pp. 9–23). Springer International Publishing. [https://doi.org/10.1007/978-3-031-04707-7\\_2](https://doi.org/10.1007/978-3-031-04707-7_2)
  19. Duguma T.A. 2023. RS and GIS analysis of the groundwater potential zones in the Upper Blue Nile River Basin, Ethiopia. *Journal of Hydrology: Regional Studies*, 46(October 2021), 101344. <https://doi.org/10.1016/j.ejrh.2023.101344>
  20. El Jazouli A., Barakat A., Khellouk R. 2019. GIS-multicriteria evaluation using AHP for landslide susceptibility mapping in Oum Er Rbia high basin (Morocco). *Geoenvironmental Disasters*, 6(1). <https://doi.org/10.1186/s40677-019-0119-7>
  21. FAO-UNESCO. 1977. FAO-UNESCO soil map of the world, 1:5000000. Africa. *Fao Soil Bulletin*, VI(1), 299.
  22. FAO & IIASA. 2023. Harmonized World Soil Database version 2.0. Rome and Laxenburg. <https://doi.org/10.4060/cc3823en>
  23. Faouzi E., Arioua A., Hssaisoune M., Boudhar A., Elaloui A., Karaoui I. 2022. Sensitivity analysis of CN using SCS-CN approach, rain gauges and TRMM satellite data assessment into HEC-HMS hydrological model in the upper basin of Oum Er Rbia, Morocco. *Modeling Earth Systems and Environment*, 8(4), 4707–4729. <https://doi.org/10.1007/s40808-022-01404-8>
  24. Ghosh A., Adhikary P.P., Bera B., Bhunia G.S., Shit P.K. 2022. Assessment of groundwater potential zone using MCDA and AHP techniques: case study from a tropical river basin of India. *Applied Water Science*, 12(3), 1–22. <https://doi.org/10.1007/s13201-021-01548-5>
  25. Hssaisoune M., Bouchaou L., Sifeddine A., Bouimtarhan I., Chehbouni A. 2020. Moroccan groundwater resources and evolution with global climate changes. *Geosciences* (Switzerland), 10(2). <https://doi.org/10.3390/geosciences10020081>
  26. Hussein A.A., Govindu V., Nigusse A.G.M. 2017. Evaluation of groundwater potential using geospatial techniques. *Applied Water Science*, 7(5), 2447–2461. <https://doi.org/10.1007/s13201-016-0433-0>
  27. Ifediegwu S.I. 2022. Assessment of groundwater potential zones using GIS and AHP techniques: a case study of the Lafia district, Nasarawa State, Nigeria. *Applied Water Science*, 12(1), 1–17. <https://doi.org/10.1007/s13201-021-01556-5>
  28. Kumar M., Singh P., Singh P. 2023. Machine learning and GIS-RS-based algorithms for mapping the groundwater potentiality in the Bundelkhand region, India. *Ecological Informatics*, 74, 101980. <https://doi.org/10.1016/j.ecoinf.2023.101980>
  29. Lentswe G.B., and Molwalefhe L. 2020. Delineation of potential groundwater recharge zones using analytic hierarchy process-guided GIS in the semi-arid Motloutse watershed, eastern Botswana. *Journal of Hydrology: Regional Studies*, 28(Jan), 100674. <https://doi.org/10.1016/j.ejrh.2020.100674>
  30. Machiwal D., Jha M.K., Mal B.C. 2011. Assessment of groundwater potential in a Semi-Arid region of India using remote sensing, GIS and MCDM techniques. *Water Resources Management*, 25(5), 1359–1386. <https://doi.org/10.1007/s11269-010-9749-y>
  31. Mallick J., Khan R.A., Ahmed M., Alqadhi S.D., Alsubih M., Falqi I., Hasan M.A. 2019. Modeling groundwater potential zone in a Semi-Arid region of Aseer using Fuzzy-AHP and geoinformation techniques. *Water*, 11(12), 2656. <https://doi.org/10.3390/w11122656>
  32. Mandal K.K., Ranjan A., Dharanirajan K. 2021. Delineation of groundwater potential zones (GWPZ)

- of Port Blair, Andaman Islands, India, using multi influencing factors (MIF) method and geospatial techniques. *Remote Sensing Applications: Society and Environment*, 24(September), 100631. <https://doi.org/10.1016/j.rsase.2021.100631>
33. Mandal P., Saha J., Bhattacharya S., Paul S. 2021. Delineation of groundwater potential zones using the integration of geospatial and MIF techniques: a case study on Rarh region of West Bengal, India. *Environmental Challenges*, 5(November), 100396. <https://doi.org/10.1016/j.envc.2021.100396>
  34. Masroor M., Sajjad H., Kumar P., Saha T.K., Rahman M.H., Choudhari P., Kulimushi L.C., Pal S., Saito O. 2023. Novel ensemble machine learning modeling approach for groundwater potential mapping in Parbhani District of Maharashtra, India. *Water*, 15(3), 419. <https://doi.org/10.3390/w15030419>
  35. Mays L.W. 2013. Groundwater resources sustainability: past, present, and future. *Water Resources Management*, 27(13), 4409–4424. <https://doi.org/10.1007/s11269-013-0436-7>
  36. Megdal S.B. 2018. Invisible water: the importance of good groundwater governance and management. *Npj Clean Water*, 1(1), 1–5. <https://doi.org/10.1038/s41545-018-0015-9>
  37. Mengistu T.D., Chung I.M., Kim M.G., Chang S.W., Lee J.E. 2022. Impacts and implications of land use land cover dynamics on groundwater recharge and surface runoff in East African Watershed. *Water (Switzerland)*, 14(13). <https://doi.org/10.3390/w14132068>
  38. Moore I.D., Grayson R.B., Ladson A.R. 1991. Digital terrain modelling: a review of hydrological, geomorphological, and biological applications. *Hydrological Processes*, 5(1), 3–30. <https://doi.org/10.1002/hyp.3360050103>
  39. Morgan H., Madani A., Hussien H.M., Nassar T. 2023. Using an ensemble machine learning model to delineate groundwater potential zones in desert fringes of East Esna-Idfu area, Nile valley, Upper Egypt. *Geoscience Letters*, 10(1). <https://doi.org/10.1186/s40562-023-00261-2>
  40. Muavhi N., Thamaga K.H., Mutoti M.I. 2022. Mapping groundwater potential zones using relative frequency ratio, analytic hierarchy process and their hybrid models: case of Nzhelele-Makhado area in South Africa. *Geocarto International*, 37(21), 6311–6330. <https://doi.org/10.1080/10106049.2021.1936212>
  41. Muñoz Sabater J. (Copernicus C.C.S. (C3S) C.D.S. (CDS)). 2019. ERA5-Land monthly averaged data from 1981 to present. <https://doi.org/10.24381/cds.68d2bb30>
  42. Oudra I., and Talks P. 2019. FAO/WB Cooperative Programme : Nationally Determined Contribution Support on the Groundwater, Energy and Food Security Nexus in Morocco.
  43. Ouma Y.O., and Tateishi R. 2014. Urban flood vulnerability and risk mapping using integrated multi-parametric AHP and GIS: Methodological overview and case study assessment. *Water (Switzerland)*, 6(6), 1515–1545. <https://doi.org/10.3390/w6061515>
  44. Ozegin K.O., Ilugbo S.O., Ogunseye T.T. 2023. Groundwater exploration in a landscape with heterogeneous geology: An application of geospatial and analytical hierarchical process (AHP) techniques in the Edo north region, in Nigeria. *Groundwater for Sustainable Development*, 20(October 2022), 100871. <https://doi.org/10.1016/j.gsd.2022.100871>
  45. Patra S., Mishra P., Mahapatra S.C. 2018. Delineation of groundwater potential zone for sustainable development: A case study from Ganga Alluvial Plain covering Hooghly district of India using remote sensing, geographic information system and analytic hierarchy process. *Journal of Cleaner Production*, 172, 2485–2502. <https://doi.org/10.1016/j.jclepro.2017.11.161>
  46. Pradhan R.M., Guru B., Pradhan B., Biswal T.K. 2021. Integrated multi-criteria analysis for groundwater potential mapping in Precambrian hard rock terranes (North Gujarat), India. *Hydrological Sciences Journal*, 66(6), 961–978. <https://doi.org/10.1080/02626667.2021.1906427>
  47. Radulović M., Brdar S., Mesaroš M., Lukić T., Savić S., Basarin B., Crnojević V., Pavić D. 2022. Assessment of groundwater potential zones using GIS and fuzzy AHP techniques – A case study of the Titel mMunicipality (Northern Serbia). *ISPRS International Journal of Geo-Information*, 11(4). <https://doi.org/10.3390/ijgi11040257>
  48. Rahman M.M., Althobiani F., Shahid S., Virdis S.G.P., Kamruzzaman M., Rahaman H., Momin M.A., Hosain M.B., Ghandourah E.I. 2022. GIS and remote sensing-based multi-criteria analysis for delineation of groundwater potential zones: A case study for industrial zones in Bangladesh. *Sustainability (Switzerland)*, 14(11). <https://doi.org/10.3390/su14116667>
  49. Rahmati O., Nazari Samani A., Mahdavi M., Pourghasemi H.R., Zeinivand H. 2015. Groundwater potential mapping at Kurdistan region of Iran using analytic hierarchy process and GIS. *Arabian Journal of Geosciences*, 8(9), 7059–7071. <https://doi.org/10.1007/s12517-014-1668-4>
  50. Saaty T.L. 1980. *The Analytic Hierarchy Process: Planning, Priority Setting, Resource Allocation*. McGraw-Hill International Book Company. <https://books.google.co.ma/books?id=Xxi7AAAAIAAJ>
  51. Saaty T.L. 1990. How to make a decision: The analytic hierarchy process. *European Journal of Operational Research*, 48(1), 9–26. [https://doi.org/10.1016/0377-2217\(90\)90057-1](https://doi.org/10.1016/0377-2217(90)90057-1)
  52. Salem A., Abduljaleel Y., Dezsó J., Lóczy D. 2023.

- Integrated assessment of the impact of land use changes on groundwater recharge and groundwater level in the Drava floodplain, Hungary. *Scientific Reports*, 13(1), 1–16. <https://doi.org/10.1038/s41598-022-21259-4>
53. Saravanan S., Saranya T., Jennifer J.J., Singh L., Selvaraj A., Abijith D. 2020. Delineation of groundwater potential zone using analytical hierarchy process and GIS for Gundihalla watershed, Karnataka, India. *Arabian Journal of Geosciences*, 13(15). <https://doi.org/10.1007/s12517-020-05712-0>
  54. Shailaja G., Kadam A.K., Gupta G., Umrikar B.N., Pawar N.J. 2019. Integrated geophysical, geospatial and multiple-criteria decision analysis techniques for delineation of groundwater potential zones in a semi-arid hard-rock aquifer in Maharashtra, India. *Hydrogeology Journal*, 27(2), 639–654. <https://doi.org/10.1007/s10040-018-1883-2>
  55. Shao Z., Huq M.E., Cai B., Altan O., Li Y. 2020. Integrated remote sensing and GIS approach using Fuzzy-AHP to delineate and identify groundwater potential zones in semi-arid Shanxi Province, China. *Environmental Modelling and Software*, 134, 104868. <https://doi.org/10.1016/j.envsoft.2020.104868>
  56. Singha S.S., Pasupuleti S., Singha S., Singh R., Venkatesh A.S. 2021. Analytic network process based approach for delineation of groundwater potential zones in Korba district, Central India using remote sensing and GIS. *Geocarto International*, 36(13), 1489–1511. <https://doi.org/10.1080/10106049.2019.1648566>
  57. Sutradhar S., Mondal P., Das N. 2021. Delineation of groundwater potential zones using MIF and AHP models: A micro-level study on Suri Sadar Sub-Division, Birbhum District, West Bengal, India. *Groundwater for Sustainable Development*, 12(March 2020), 100547. <https://doi.org/10.1016/j.gsd.2021.100547>
  58. Taher M., Mourabit T., Etebaai I., Cherkaoui Dekkaki H., Amarjoun N., Amine A., Abdelhak B., Errahmouni A., Azzouzi S. 2023. Identification of Groundwater Potential Zones (GWPZ) Using Geospatial Techniques and AHP Method: a Case Study of the Boudinar Basin, Rif Belt (Morocco). *Geomatics and Environmental Engineering*, 17(3), 83–105. <https://doi.org/10.7494/geom.2023.17.3.83>
  59. Thapa R., Gupta S., Gupta A., Reddy D. V., Kaur H. 2018. Use of geospatial technology for delineating groundwater potential zones with an emphasis on water-table analysis in Dwarka River basin, Birbhum, India. *Hydrogeology Journal*, 26(3), 899–922. <https://doi.org/10.1007/s10040-017-1683-0>
  60. Tiwari A., Ahuja A., Vishwakarma B.D., Jain K. 2019. Groundwater Potential Zone (GWPZ) for Urban Development Site Suitability Analysis in Bhopal, India. *Journal of the Indian Society of Remote Sensing*, 47(11), 1793–1815. <https://doi.org/10.1007/s12524-019-01027-0>
  61. Trabelsi F., Bel Hadj Ali S., Lee S. 2022. Comparison of Novel Hybrid and Benchmark Machine Learning Algorithms to Predict Groundwater Potentiality: Case of a Drought-Prone Region of Medjerda Basin, Northern Tunisia. *Remote Sensing*, 15(1), 152. <https://doi.org/10.3390/rs15010152>
  62. Upwanshi M., Damry K., Pathak D., Tikle S., Das S. 2023. Delineation of potential groundwater recharge zones using remote sensing, GIS, and AHP approaches. *Urban Climate*, 48(January), 101415. <https://doi.org/10.1016/j.uclim.2023.101415>
  63. Weiss a. 2001. Topographic position and landforms analysis. Poster Presentation, ESRI User Conference, San Diego, CA, 64, 227–245. <http://scholar.google.com/scholar?hl=en&btnG=Search&q=intitle:Topographic+Position+and+Landforms+Analysis#0>
  64. World Bank Group. 2017. *Managing Urban Water Scarcity in Morocco* (Issue November).
  65. World Bank Group. 2021. *Climate Risk Country Profile: Morocco*. In *The World Bank Group (WBG)*.
  66. Yadav B., Malav L.C., Jangir A., Kharia S.K., Singh S. V., Yeasin M., Nogiya M., Meena R.L., Meena R.S., Tailor B.L., Mina B.L., Alhar M.S.O., Jeon B.-H., Cabral-Pinto M.M.S., Yadav K.K. 2023. Application of analytical hierarchical process, multi-influencing factor, and geospatial techniques for groundwater potential zonation in a semi-arid region of western India. *Journal of Contaminant Hydrology*, 253(December 2022), 104122. <https://doi.org/10.1016/j.jconhyd.2022.104122>
  67. Yesilnacar E., and Topal T. 2005. Landslide susceptibility mapping: A comparison of logistic regression and neural networks methods in a medium scale study, Hendek region (Turkey). *Engineering Geology*, 79(3–4), 251–266. <https://doi.org/10.1016/j.enggeo.2005.02.002>
  68. Yifru B.A., Mitiku D.B., Tolera M.B., Chang S.W., Chung I.-M. 2020. Groundwater Potential Mapping Using SWAT and GIS-Based Multi-Criteria Decision Analysis. *KSCE Journal of Civil Engineering*, 24(8), 2546–2559. <https://doi.org/10.1007/s12205-020-0168-1>
  69. Zamani M.G., Moridi A., Yazdi J. 2022. Groundwater management in arid and semi-arid regions. *Arabian Journal of Geosciences*, 15(4), 362. <https://doi.org/10.1007/s12517-022-09546-w>
  70. Zanaga D., Van De Kerchove R., Daems D., De Keersmaecker W., Brockmann C., Kirches G., Wevers J., Cartus O., Santoro M., Fritz S., Lesiv M., Herold M., Tsensbazar N.E., Xu P., Ramoino F., Arino O. 2022. *ESA WorldCover 10 m 2021 v200*. In *Meteosat Second Generation Evapotranspiration (MET)*. <https://doi.org/10.5281/ZENODO.7254221>